Be-composition effect on structure, electronic and optical properties of $Be_xZn_{1-x}O$ alloys*

Lü Bing(吕 兵)[a)b)], Zhou Xun(周 勋)[b)c)], Linghu Rong-Feng(令狐荣锋)[a)b)], Wang Xiao-Lu(王晓璐)[a)b)], and Yang Xiang-Dong(杨向东)[a)†]

[a)] *Institute of Atomic and Molecular Physics, Sichuan University, Chengdu* 610065, *China*
[b)] *School of Physics and Electronic Science, Guizhou Normal University, Guiyang* 550001, *China*
[c)] *College of Science, Guizhou University, Institute of New Optoelectronic Materials and Technology, Guizhou University, Guiyang* 550025, *China*

(Received 6 September 2010; revised manuscript received 22 October 2010)

This paper carries out first principles calculation of the structure, electronic and optical properties of $Be_xZn_{1-x}O$ alloys based on the density-functional theory for the compositions $x = 0.0, 0.25, 0.5, 0.75, 1.0$. The lattice constants deviations of alloys obey Vegard's law well. The $Be_xZn_{1-x}O$ alloys have the direct band gap (Γ–Γ) character, and the bowing coefficients are less than the available theoretical values. Moreover, it investigates in detail the optical properties (dielectric functions, absorption spectrum and refractive index) of these ternary mixed crystals. The obtained results agree well with the available theoretical and experimental values.

Keywords: alloys, optical properties, generalized gradient approximation, $Be_xZn_{1-x}O$

PACS: 61.66.Dk, 78.20.Ci, 71.15.Mb, 77.55.hf **DOI:** 10.1088/1674-1056/20/3/036104

1. Introduction

The ZnO is a kind of wide band gap semiconductors and an attractive material due to its use in ultraviolet optoelectronic applications, solar cell,[1] sensors,[2] nanolaser,[3,4] etc. To produce high-efficiency ZnO-based light emitting devices, the critical step is the fabrication of quantum wells and superlattices of ZnO-based semiconductor alloy by mixing with materials with even larger band gaps. Up to now, the investigations of ZnO-based semiconductor alloy focus on $Cd_xZn_{1-x}O$, $Mg_xZn_{1-x}O$ and $Be_xZn_{1-x}O$. However, obvious differences exist among these alloys. Due to the large lattice mismatch between ZnO (B4) and MgO (B1), CdO (B1), $Mg_xZn_{1-x}O$ and $Cd_xZn_{1-x}O$ alloys have wurtzite structure at modest Mg (Cd) composition. The $Mg_xZn_{1-x}O$ crystal phase segregation is found at $x > 1/3$, it was theoretically predicted[5] and experimentally confirmed.[6] Also the upper limit of Cd composition is 0.25 for $Cd_xZn_{1-x}O$ alloys.[7–9] Furthermore, doping Cd into ZnO can reduce the band gap, and band gap can increase by doping Mg. However, $Be_xZn_{1-x}O$ have advantages over $Mg_xZn_{1-x}O$ and $Cd_xZn_{1-x}O$. Because BeO has the same hexagonal wurtzite structure as ZnO, phase segregation is not detected in $Be_xZn_{1-x}O$ alloys.

In recent years, density functional theory (DFT) based first principles methods have gained increasing popularity due to their high accuracy and efficiency.[10–12] Amrani *et al.*[13] investigated the structural, electronic and thermodynamic properties of $Zn_{1-x}Mg_xO$ alloys in the cubic phase using the full potential linearized augmented plane wave (FP-LAPW) method. Rozale *et al.*[14] used the FP-LAPW method to study the ordered structures of $Zn_{1-x}Cd_xO$ alloys. Recently, Fan *et al.*[15] and Duan *et al.*[16] studied the electronic properties and piezoelectricity of $Be_xZn_{1-x}O$. However, only very few theoretical investigations on optical properties of $Be_xZn_{1-x}O$ alloys have been reported in the literature.

In this work, the optical properties are investigated in detail for $Be_xZn_{1-x}O$ alloys. The results obtained are in good agreement with the available experimental data and other theoretical calculation. In Section 2, a brief description of computational method is given. The results of optical properties are discussed in Section 3. The results obtained are also compared with other available theoretical results and existing

*Project supported by the National Natural Science Foundation of China (Grant Nos. 10974139 and 10964002), the Specialized Research Fund for the Doctoral Program of Higher Education of China (Grant No. 20050610010), the Science-Technology Foundation of Guizhou Province of China (Grant Nos. [2009]2066, [2009]06 and [2010]2146), the Project of Aiding Elites' Research Condition of Guizhou Province of China (Grant No. TZJF-2008-42).

†Corresponding author. E-mail: xdyang@scu.edu.cn

© 2011 Chinese Physical Society and IOP Publishing Ltd

experimental data. Finally, the summary of our main results and conclusion are given in Section 4.

2. Computational methods

All calculations on $Be_xZn_{1-x}O$ alloys are carried out based on the DFT and plane-wave pseudopotential methods, which are implemented in the first-principles calculation programme CASTEP code. The electronic exchange and correlation functions are treated within DFT via generalized gradient approximation (GGA) with the Perdew–Wang functional.[17] Interactions of electrons with ion cores are represented by the ultrasoft pseudopotential. Electronic states of Zn 3d and O 2s are treated as valence states because their orbit energies are relatively high. According to the special quasirandom structures (SQS) approach,[18] the $Be_xZn_{1-x}O$ (x = 0.0, 0.25, 0.5, 0.75, 1.0) structures can be obtained by replacing 1 to 8 Zn atoms with Be in the 2×2×1 wurtzite ZnO supercell. The convergence of the total energy with respect to both k-point sampling and plane-wave cutoff energy is carefully examined. The plane-wave basis set with an energy cut-off 680.0 eV has been applied, and the 6×6×8 Monkhorst–Pack mesh has been used for the Brillouin-zone (BZ) k-point sampling. The self-consistent convergence of the total energy is at 5.0×10^{-7} eV/atom.

In addition, to investigate electronic and optical properties accurately, more k-points are needed and a denser 10×10×12 k-points are generated. Furthermore, the number of conduction bands is also an important parameter in the calculation, which defines the energy range covered and determines the accuracy of the Kramers–Kronig transform. In present work, 20 empty bands in addition to the occupied bands are included.

3. Results and discussions

3.1. Structural properties

For the considered structures, we perform the structural optimisation by minimizing the total energy with respect to the cell parameters. Table 1 shows the lattice constants (a, c) and bulk modulus (B) for each x of $Be_xZn_{1-x}O$ alloys along with the other experimental and theoretical values. The calculated lattice parameters are a = 3.249 Å, c = 5.205 Å (1 Å = 0.1 nm) for ZnO and a = 2.752 Å, c = 4.456 Å for BeO in wurtzite phase. It is clear that our results are in reasonable agreement with experimental values[19,20] and literature.[16] These results indicate that the method used in our case is reasonable.

Table 1. The lattice constants (a, c) and bulk modulus B of $Be_xZn_{1-x}O$ alloys.

structures	a/Å	c/Å	B/GPa
ZnO	3.249, 3.25[a], 3.199[b]	5.205, 5.21[a], 5.168[b]	155.95, 160.2[b], 160.2[d]
$Be_{0.25}Zn_{0.75}O$	3.133	5.061	168.42
$Be_{0.5}Zn_{0.5}O$	2.985	4.861	183.63
$Be_{0.75}Zn_{0.25}O$	2.888	4.67	201.68
BeO	2.752, 2.717[b], 2.698[c]	4.456, 4.413[b], 4.376[c]	221.06, 224.4[a], 223[b]

[a] From Ref. [19], [b] From Ref. [16], [c] From Ref. [20], [d] From Ref. [21].

According to the Vegard's Law,[22] physical properties of an alloy $A_xB_{1-x}C$ can be obtained, in good approximation, by a linear relation between the physical property $F(A_xB_{1-x}C)$ and the composition x, the relation is as follows:

$$F(A_xB_{1-x}C) = xF_{AC} + (1-x)F_{BC}, \qquad (1)$$

where F_{AC} and F_{BC} are physical properties of the end-point compounds. However, many alloys deviate from linear behaviour. A general form of their behaviour is expressed by a semi empirical quadratic relationship[23]

$$F(A_xB_{1-x}C) = xF_{AC} + (1-x)F_{BC} + bx(1-x), \qquad (2)$$

where b is the bowing parameter which accounts for the deviation from a linear behaviour.

The composition dependence of the calculated equilibrium lattice parameter for $Be_xZn_{1-x}O$ alloys are shown in Figs. 1 and 2. It is found that the deviation of the optimised lattice constants from linearity is relatively small. Due to the small mismatching between the lattice constants of ZnO and BeO, the small bowing parameter b is calculated to be 0.026 Å and 0.181 Å for a and c, respectively. Moreover, since the

ionic radius of Be^{2+} is smaller than that of Zn^{2+}, the lattice constants a and c decrease with increasing Be concentration. This causes the material to be more rigid, and therefore it increases the bulk modulus of $Be_xZn_{1-x}O$ alloys, as shown in Table 1.

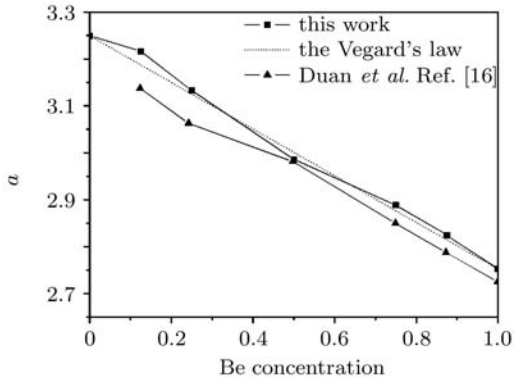


Fig. 1. The lattice constant a versus Be concentration.

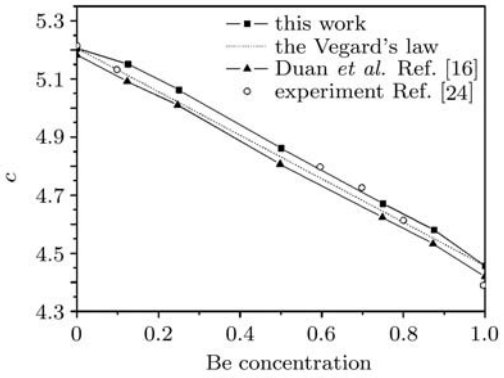


Fig. 2. The lattice constant c versus Be concentration.

3.2. Electronic properties

We give the band structures for $Be_xZn_{1-x}O$ as shown in Figs. 3–7. After substituting parts of Zn atoms with Be atoms in the ZnO compounds, we find that $Be_xZn_{1-x}O$ have the direct band gap (Γ–Γ) character. Moreover, the band gap of all $Be_xZn_{1-x}O$ shows an increasing feature varying with the molar fraction x. Figure 8 is plotted to show the band gaps at different Be composition in comparison with Ref. [15] and experimental[24] results. The direct band gap shows the relation as follows:

$$E_g(\mathrm{ZnO}) < E_g(\mathrm{Be_{0.25}Zn_{0.75}O}) < E_g(\mathrm{Be_{0.5}Zn_{0.5}O}) < E_g(\mathrm{Be_{0.75}Zn_{0.25}O}) < E_g(\mathrm{BeO}).$$

Electronic structure calculations can predict also the nature and location of interband transitions in a crystal, which will assist the experimentalists in identifying the peaks in the optical spectra obtained by either reflectance or photoelectron spectroscopy. Based on the electronic band structure shown in Figs. 3–8, the results of the interband transitions at Γ A, H, K, M and L points are listed in Table 2, together with the experimental data and other theoretical results.

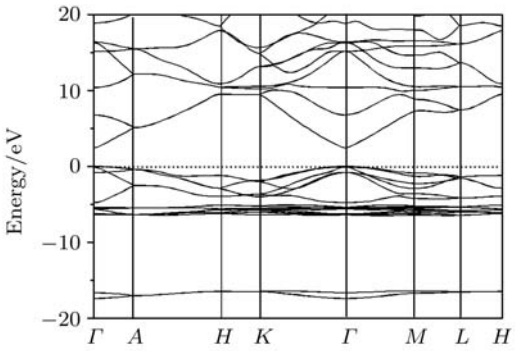


Fig. 3. Energy band structure of ZnO.

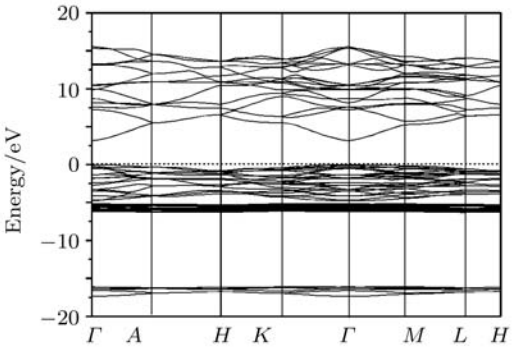


Fig. 4. Energy band structure of Zn_6Be_2O.

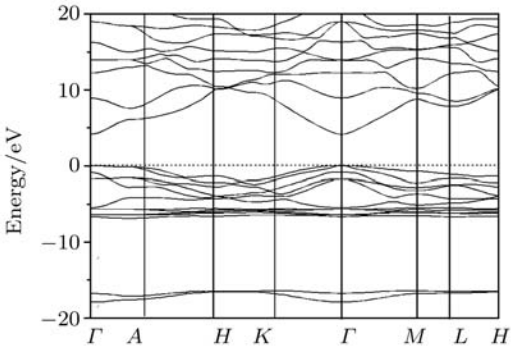


Fig. 5. Energy band structure of Zn_4Be_4O.

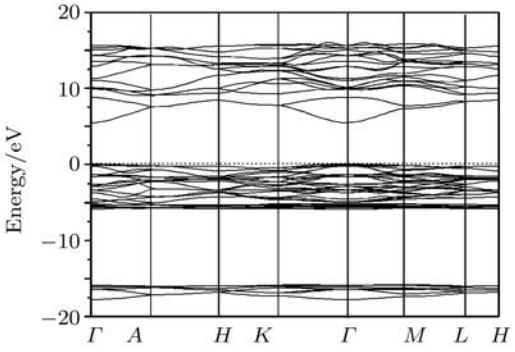


Fig. 6. Energy band structure of Zn_2Be_6O.

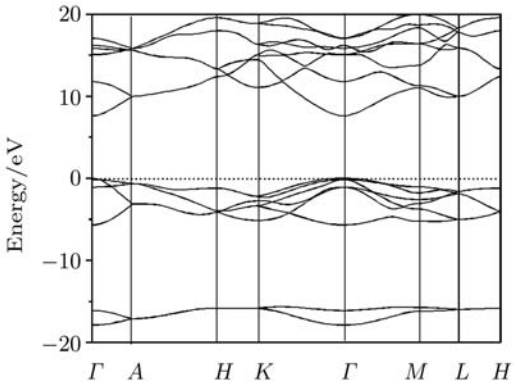


Fig. 7. Energy band structure of BeO.

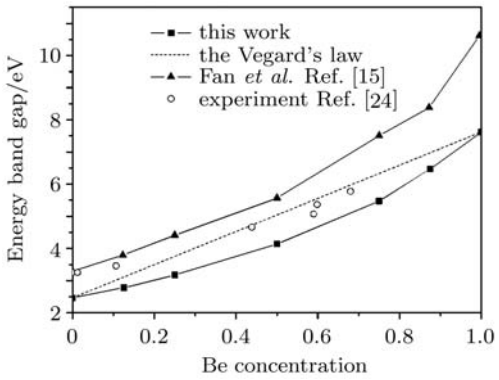


Fig. 8. Composition dependence of the band gap.

Table 2. The calculated band-gap of $Be_xZn_{1-x}O$ alloys.

structures	Γ–Γ	Γ–A	Γ–H	Γ–K	Γ–M	Γ–L
ZnO	2.47, 0.812[a], 3.44[b], 4.23[c]	4.97	9.47	9.45	7.16	7.39
$Be_{0.25}Zn_{0.75}O$	3.12	5.57	6.55	5.54	5.27	6.38
$Be_{0.5}Zn_{0.5}O$	4.09	6.11	10.02	8.74	8.81	7.83
$Be_{0.75}Zn_{0.25}O$	5.55	7.54	8.44	7.74	7.33	8.23
BeO	7.56, 10.7[d], 7.0[e]	9.95	12.38	11.03	10.92	9.86

[a] Ref. [16], [b] Experimental value from Ref. [25], [c] Ref. [26], [d] Experimental value from Ref. [27], [e] Ref. [28].

The experimental data show that the band gap E_g of the alloy $A_xB_{1-x}C$ is not linear with the molar fraction x. In most cases the band gaps show a quadratic dependence on x,[29]

$$E_g(A_xB_{1-x}C) = xE_g(AC) + (1-x)E_g(BC) - bx(1-x), \quad (3)$$

where b is the bowing parameter. The calculated bowing coefficients are listed in Table 3 for $Be_xZn_{1-x}O$. The bowing coefficient b is composition dependent and increases slowly with increasing x. Our results are less than the available theoretical values.[16]

Table 3. The calculated band-gap bowing coefficients of $Be_xZn_{1-x}O$ alloys.

	0.125	0.25	0.5	0.75	0.875
b/eV	3.028	3.058	3.584	4.546	4.551
	3.984[a]	3.926[a]	5.625[a]	6.804[a]	12.286[a]

[a] From Ref. [16].

3.3. Optical properties

The complex dielectric function $\varepsilon(\omega)$ can be used to describe the linear response of the system to electromagnetic radiation, which relates to the interaction of photons with electrons, it has the form $\varepsilon(\omega) = \varepsilon_1(\omega) + \varepsilon_2(\omega)$. It is well known that the imaginary part $\varepsilon_2(\omega)$ of the dielectric function can be calculated with the momentum matrix elements between the occupied and unoccupied wavefunctions within the selection rules, and the real part $\varepsilon_1(\omega)$ of the dielectric function follows from the Kramers–Kronig relations:

$$\varepsilon_1(\omega) = 1 + \frac{2}{\pi}\int_0^\infty \frac{\varepsilon_2(\omega')\omega' \mathrm{d}\omega'}{\omega'^2 - \omega^2}, \quad (4)$$

$$\varepsilon_2(\omega) = \frac{Ve^2}{2\pi\hbar m^2\omega^2}\int \mathrm{d}^3k \sum_{nn'} |\langle kn|p|kn'\rangle|^2 f(kn) \times [1 - f(kn')]\partial(E_{kn} - E_{kn'} - \hbar\omega), \quad (5)$$

where $\hbar\omega$ is the energy of the incident photon, p is the momentum operator, $|kn\rangle$ is the eigenfunction with eigenvalue E_{kn} and $f(kn)$ is the Fermi distribution function.

All the other optical constants can be derived from $\varepsilon_2(\omega)$ and $\varepsilon_1(\omega)$, such as absorption coefficient $\alpha(\omega)$ and refractive index $n(\omega)$,

$$n(\omega) = \frac{1}{\sqrt{2}}\left[\sqrt{\varepsilon_1^2(\omega) + \varepsilon_2^2(\omega)} + \varepsilon_1\right]^{1/2}, \quad (6)$$

$$\alpha(\omega) = \sqrt{2}\omega\left[\sqrt{\varepsilon_1^2(\omega) + \varepsilon_2^2(\omega)} - \varepsilon_1(\omega)\right]^{1/2}. \quad (7)$$

Using Eqs. (4)–(7), we calculate dielectric functions ($\varepsilon_1(\omega)$, $\varepsilon_2(\omega)$), refractive index $n(\omega)$ and absorption coefficient $\alpha(\omega)$.

The calculated optical properties at the equilibrium lattice constant are illustrated in detail in the present work. The results have been presented in Figs. 9–16. It is well known that the imaginary part of the dielectric function $\varepsilon_2(\omega)$ can be treated by the real transitions between occupied and unoccupied electronic states. The $\varepsilon_1(\omega)$ and $\varepsilon_2(\omega)$ are shown in Figs. 9–12 for ZnO and BeO. The remarkable anisotropic behaviours can be clearly elucidated in the $\varepsilon_1(\omega)$ and $\varepsilon_2(\omega)$ functions along different polarisation directions in ZnO. The dielectric constants $\varepsilon_1(0)$ are 5.37 and 9.43 corresponding to the polarisation directions (001) and (100), respectively. For BeO, the dielectric property is almost isotropic with the values of the dielectric constant $\varepsilon_1(0)$ of 3.01 and 3.13 corresponding to the parallel and perpendicular directions to the c-axis, respectively. The respective experimental values are 2.99 and 2.95 corresponding to parallel and perpendicular directions to the c-axis for BeO.[30] The agreement among them is good.

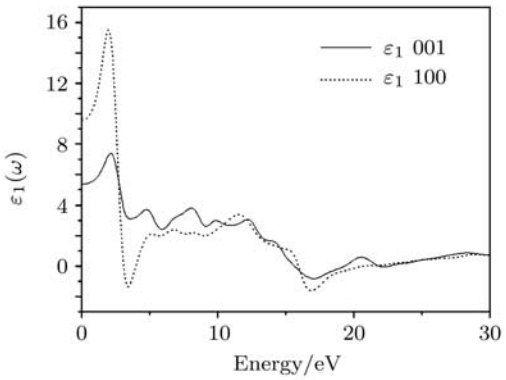


Fig. 9. The $\varepsilon_1(\omega)$ function of ZnO along polarisation directions (001) and (100).

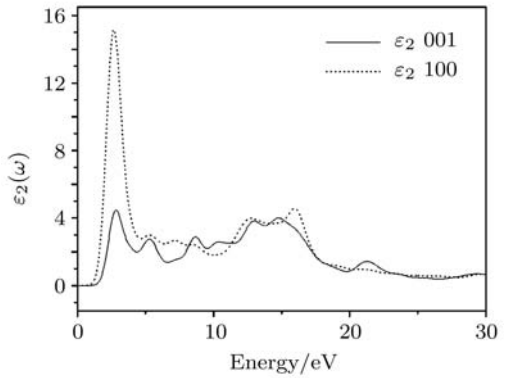


Fig. 10. The $\varepsilon_2(\omega)$ function of ZnO along polarisation directions (001) and (100).

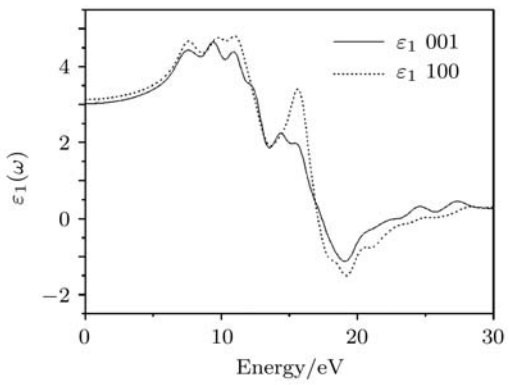


Fig. 11. The $\varepsilon_1(\omega)$ function of BeO along polarisation directions (001) and (100).

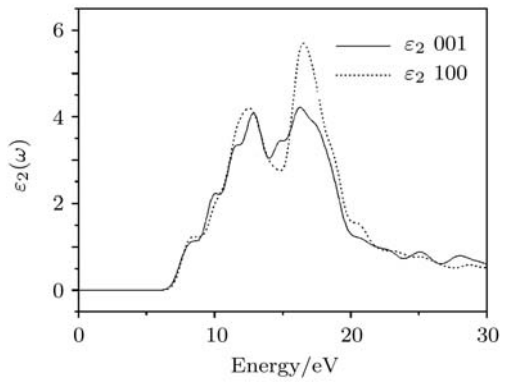


Fig. 12. The $\varepsilon_2(\omega)$ function of BeO along polarisation directions (001) and (100).

The real part $\varepsilon_1(\omega)$ and imaginary part $\varepsilon_2(\omega)$ for $Be_xZn_{1-x}O$ are displayed in Figs. 13 and 14, respectively, where the solid lines represent the dielectric function along polarisation direction (001), the dotted lines represent the dielectric function along polarisation direction (100) and the dark gray lines represent the values reported in the literatures[31,32] for ZnO and BeO along polarisation direction (001). It is clear that the calculated values of ZnO and BeO are in line with the literatures[31,32] and the previous calculated parameters are reasonable for the investigation of the optical properties of $Be_xZn_{1-x}O$. An important quantity of $\varepsilon_1(\omega)$ is the zero frequency limit $\varepsilon_1(0)$, which depends on the band gap as $\varepsilon_1(0) \approx 1 + (\hbar\omega_p/E_g)^2$, where ω_p is the plasma frequency at which $\varepsilon_1(\omega)$ passes through zero.[33] The $Be_xZn_{1-x}O$ has the similar characteristic in the static dielectric constant $\varepsilon_1(0)$ changing with the molar fraction x along polarisation direction (001) or (100). Our calculated static dielectric constants for $Be_xZn_{1-x}O$ are 5.49, 3.98, 3.69, 3.15 and 3.02 along polarisation direction (001) and 9.47, 4.78, 4.01, 3.33 and 3.09 along polarisation direction (100) corresponding to $x = 0.0$, 0.25, 0.50, 0.75 and

1.0, respectively. It indicates that the static dielectric constants reduce with increasing Be concentration. In the range 0.0–10.0 eV, as x increases, the first strong peak in $\varepsilon_1(\omega)$ shifts towards higher incident photon energy, which varies from 2.06 eV in ZnO to 7.51 eV in BeO along polarisation direction (001) and from 1.99 eV in ZnO to 7.57 eV in BeO along polarisation direction (100).

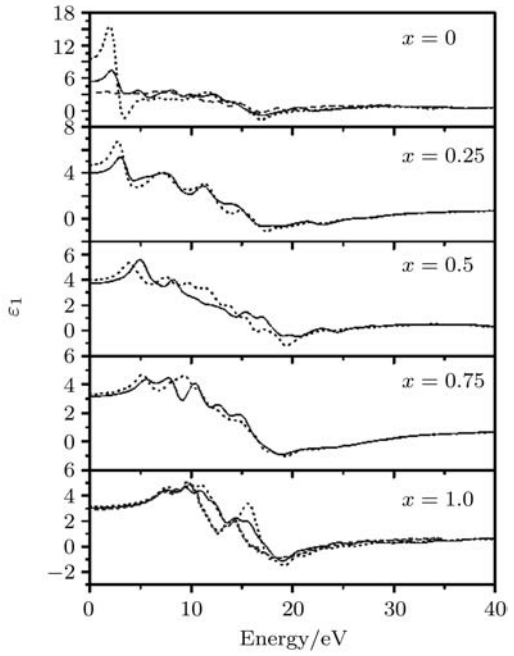


Fig. 13. The $\varepsilon_1(\omega)$ function of $Be_xZn_{1-x}O$ alloys along polarisation directions (001) and (100).

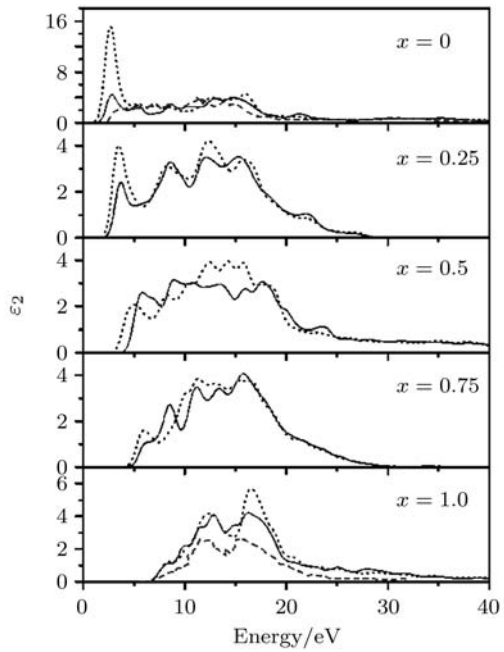


Fig. 14. The $\varepsilon_2(\omega)$ function of $Be_xZn_{1-x}O$ alloys along polarisation directions (001) and (100).

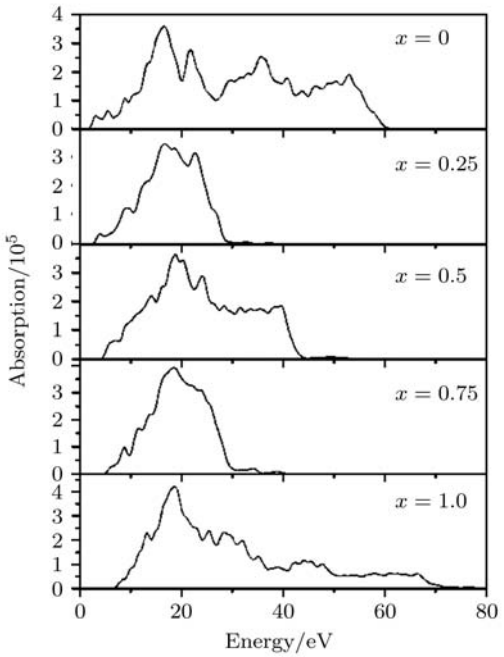


Fig. 15. Varieties of absorption of $Be_xZn_{1-x}O$ alloys along (001) direction.

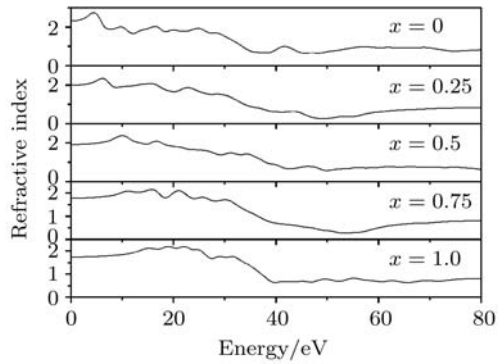


Fig. 16. Varieties of refractive index of $Be_xZn_{1-x}O$ alloys along (001) direction.

From Fig. 14, it is noted that ZnO has a strong absorption region which starts from 1.45 eV to 19.37 eV along polarisation direction (100) and from 1.19 eV to 18.14 eV along polarisation direction (100), while BeO has less region of strong absorption. The first critical points of $\varepsilon_2(\omega)$ occur at 1.86, 2.69, 3.95, 5.28 and 7.18 along polarisation direction (001) and 1.48, 2.37, 2.91, 4.75 and 7.18 along polarisation direction (100) for $Be_xZn_{1-x}O$ corresponding to $x = 0.0$, 0.25, 0.50, 0.75 and 1.0, respectively, and are attributed to the direct optical transitions occurring at Γ–Γ. Moreover, with the increasing Be concentration, the anisotropic behaviours of the $\varepsilon_1(\omega)$ and $\varepsilon_2(\omega)$ functions reduce obviously along different polarisation directions.

The variations of absorption, refractive index with increasing concentration of Be in $Be_xZn_{1-x}O$ are shown in Figs. 15 and 16 along polarisation direction

(001). The shape of the optical absorption is the most important, which shows a sharp onset followed by an almost plateau. The absorption edge starts at about 1.41, 1.93, 3.86, 4.38 and 6.18 eV, respectively. It is noticed that a high absorption peak occurs in ZnO in the energy range of 11.92–20.17 eV and the peak shifts towards lower energy as the concentration of Be increases. In the area of absorption band, there are six main peaks, which are associated with interband transitions from the top of the valence band to the bottom of the conduction band at Γ, A, H, K, M and L points, respectively. The refractive index of material is an important optical parameter, which is often required to interpret various types of spectroscopic data. It is related to the density and the local polarisability of these entities.[34] The refractive index of a semiconductor $n(E)$ is computed through the real dielectric function $n\sqrt{\varepsilon_1}$. The part of the refractive index is presented in Fig. 16 and refractive indices $n(0)$ for $Be_xZn_{1-x}O$ are found to be 2.35, 1.98, 1.91, 1.79 and 1.73 with the increasing x, respectively. The index of refraction was measured to be 1.72 along c-axes for BeO,[35] showing an excellent agreement with our calculated value.

4. Conclusions

In summary, the equilibrium structure, electronic and optical properties of $Be_xZn_{1-x}O$ alloys are discussed in detail. The obtained lattice constants indicated a close agreement with the reported experimental values and literature data. Moreover, the deviations of lattice constants of alloys obey Vegard's law well. With increasing Be content, $Be_xZn_{1-x}O$ has the direct band gap (Γ–Γ) character, and the bowing coefficients b are less than the available theoretical values.[16] The remarkable anisotropic behaviours can be clearly elucidated in the $\varepsilon_1(\omega)$ and $\varepsilon_2(\omega)$ functions along different polarisation directions in ZnO, while the dielectric property is almost isotropic for BeO. Moreover, with the increasing Be concentration, The anisotropic behaviours of $Be_xZn_{1-x}O$ reduce obviously in the $\varepsilon_1(\omega)$ and $\varepsilon_2(\omega)$ functions along different polarisations directions. For polarisation direction (001), the absorption edge starts at about 1.41, 1.93, 3.86, 4.38 and 6.18 eV, respectively. In the area of absorption band, there are six main peaks, which are associated with interband transitions from the top of the valence band to the bottom of the conduction band at Γ, A, H, K, M and L points, respectively. The refractive indices $n(0)$ for $Be_xZn_{1-x}O$ are found to be 2.35, 1.98, 1.91, 1.79 and 1.73 with the increasing x, respectively. The calculated value of BeO shows an excellent agreement with that in Ref. [35].

References

[1] Keis K, Magnusson E, Lindstrom H, Lindquist S E and Hagfeldt A 2002 *Sol. Energy Mater. Sol. Cells* **73** 51

[2] Golego N, Studenikin S A and Cocivera M 2000 *J. Electron. Chem. Soc.* **147** 1592

[3] Huang M H, Mao S, Feick H, Yan H, Wu Y, Kind H, Weber E, Russo R and Yang P 2001 *Science* **292** 1897

[4] Johnson J C, Yan H, Schaller R D, Haber L H, Saykally R J and Yang P 2001 *J. Phys. Chem.* B **105** 11387

[5] Sanati M, Hart G L W and Zunger A 2003 *Phys. Rev.* B **68** 155210

[6] Ohtomo A, Kawasaki M, Ohkubo I, Koinuma H, Yasuda T and Segawa Y 1999 *Appl. Phys. Lett.* **75** 980

[7] Makino T, Segawa Y, Kawasaki M, Ohtomo A, Shiroki R, Tamura K, Yasuda T and Koinuma H 2001 *Appl. Phys. Lett.* **78** 1237

[8] Pérez J Z, Sanjosé V M, Lorenz M, Benndorf G, Heitsch S, Spemann D and Grundmann M 2006 *J. Appl. Phys.* **99** 023514

[9] Vigil O, Vaillant L, Cruz F, Santana G, Morales-Acevedo A and Contreras-Puente G 2000 *Thin Solid Films* **53** 361

[10] Yun J N, Zhang Z Y,Yan J F and Deng Z H 2010 *Chin. Phys.* B **19** 17101

[11] Yao W J, Yu Z Y and Liu Y M 2010 *Chin. Phys.* B **19** 77101

[12] Wu H P, Deng K M, Tan W S, Xiao C Y, Hu F L and Li Q X 2009 *Chin. Phys.* B **18** 5008

[13] Amrani B, Ahmed R and Hassan F El Haj 2007 *Comput. Mater. Sci.* **40** 66

[14] Rozale H, Bouhafs B and Ruterana P 2007 *Superlattice and Microst.* **42** 165

[15] Fan X F, Zhu Z X, Ong Y S, Lu Y M, Shen Z X and Kuo J L 2007 *Appl. Phys. Lett.* **91** 121121

[16] Duan Y F, Shi H L and Qin L X 2008 *Phys. Lett.* A **372** 2930

[17] Perdew J P and Wang Y 1992 *Phys. Rev.* B **45** 13244

[18] Zunger A, Wei S H, Ferreira L G and Bernsrd J E 1990 *Phys. Rev. Lett.* **65** 353

[19] Madelung O, Schultz M and Weiss H 1982 *Numerical Data and Functional and Relationships in Science and Technology* (Berlin: Springer-Verlag) p97

[20] Hazen R M and Finger L W 1986 *J. Appl. Phys.* **59** 3728

[21] Charifi Z, Baaziz H and Hussain R A 2007 *Phys. Status Solidi.* B **244** 3154

[22] Vegard L 1921 *Z. Phys.* **5** 17
[23] Hassan E H, Hashemifar F J and Akbarzadeh H 2006 *Phys. Rev.* B **73** 195202
[24] Ryua Y R, Lee T S, Lubguban J A, Corman A B, White H W, Leem J H, Han M S, Park Y S, Youn C J and Kim W J 2006 *Appl. Phys. Lett.* **88** 052103
[25] Mang A, Reimann K and Rubenacke S 1995 *Solid State Commun.* **94** 251
[26] Massidda S, Resta R, Posternak M and Baldereschi A 1995 *Phys. Rev.* B **52** 16977
[27] Griindler R, Breuer K and Tews W 1978 *Phys. Statu Solidi* (b) **86** 329
[28] Chang K J, Froyen S and Cohen M L 1983 *J. Phys.* C: *Solid State Phys.* **16** 3475
[29] Bernard J E and Zunger A 1986 *Phys. Rev.* B **34** 5992
[30] Lide D R 1991 *Handbook of Chemistry and Physics* (New York: CRC Press) p248
[31] Nazir S, Ikrama N, Amin B, Tanveer M, Shaukat A and Saeed Y 2009 *J. Phys. and Chem. of Solid.* **70** 874
[32] Groh D, Pandey R, Sahariah M B, Amzallag E, Baraille I and Rérat M 2009 *J. Phys. and Chem. of Solid.* **70** 789
[33] Penn D R 1962 *Phys. Rev.* **128** 2093
[34] Goldhahn R, Scheiner J, Shokhovets S, Frey T, Ko Ehler U, As D J and Lischkam K 1999 *Phys. Status Solidi (B)* **216** 265
[35] Yen T S, Kuo C K, Han W L, Qui Y H and Huang Y Z 1983 *J. Am. Ceram. Soc.* **66** 860